Acta Polytechnica **63**(4):227–241, 2023
https://doi.org/10.14311/AP.2023.63.0227

Published by the Czech Technical University in Prague

COMPRESSION BEHAVIOUR AND FAILURE MECHANISMS OF A SAFETY CULVERT MADE OF HOLLOW HIGH-PERFORMANCE CONCRETE BLOCKS

Petr Hála[a,*], Filip Šmejkal[b,c], Radoslav Sovják[a]

[a] *Czech Technical University in Prague, Faculty of Civil Engineering, Experimental Centre, Thákurova 7, 16629 Prague 6, Czech Republic*

[b] *Czech Technical University in Prague, Faculty of Civil Engineering, Department of Physics, Thákurova 7, 16629 Prague 6, Czech Republic*

[c] *Červenka Consulting, Na Hřebenkách 55, 15000 Prague 5, Czech Republic*

[*] corresponding author: petr.hala@fsv.cvut.cz

Abstract. The safety culvert composed of hollow high-performance concrete blocks is designed to reduce the risk of injury in the event of a collision. This work presents a new design with an opening for water flow, tests it, identifies its weaknesses, and discusses possible improvements. The numerical model is constructed, validated by experiment, and used to study the effect of design parameters on the load capacity, compression behaviour, and failure mechanisms. The response varies most markedly with the opening diameter. The failure mode changes from bending failure to concrete crushing as the diameter decreases. The effect is most pronounced for diameters less than 400 mm, where the load capacity increases by 6 kN per millimetre reduction. If a crack develops in the culvert during its service life, the first such crack will form in the top layer of blocks, followed by a crack in the opening. These areas should be monitored more closely during follow-up tests with passing vehicles.

Keywords: High-performance concrete, safety culvert, cracks, cellular structure, column load test.

1. Introduction

Cross-drainage culverts are the fifth most common type of fixed man-made object to be struck, and almost half of the injuries associated with a vehicle colliding with them are fatal or serious [1]. Currently, cross-drainage culverts are made of stone or cast concrete. A collision with such culverts is similar to a head-on collision with a solid wall because a drainage ditch directs a car that has left the road directly into the face of the culvert. The safety version of a culvert has been designed in [2] to reduce the risk of injury from a collision with such an object. It consists of brittle blocks with a cellular structure and gradually decelerates the impacting vehicle through a progressive cell fracture process.

Full-scale laboratory tests were carried out in [2] and [3] using a non-deformable flat-nosed cart to verify the ability of the blocks to gradually absorb the impact energy. The blocks were then built into the culvert, embedded in the ground, and subjected to the impact of an ordinary passenger vehicle [3]. It was found that, unlike in the case of a collision with an ordinary culvert, during the collision with the safety culvert, the crumple zone of the passenger vehicle was not crumpled, the vehicle rebound was eliminated, and a gradual deceleration of the vehicle was recorded. In [3], a culvert was built out of hollow clay blocks. Hollow blocks of high-performance concrete were used in [2]. In this study, high-performance concrete was also used as a base material due to its brittle fracture [4] and durability under harsh environmental conditions [5].

The previous studies were aimed at investigating the energy absorption capacity of the culvert, with only a marginal discussion of its load-bearing capacity. One study [3] relied on the load-bearing capacity of the individual blocks specified by the manufacturer, which they verified using only a single sample. The other [2] carried out load-bearing tests of a reduced-scale sample. The aim of the present work is to determine the load-bearing capacity of the block compositions that will be placed in the resulting structure, and thus to determine the overall load-bearing capacity.

Various studies have provided valuable insights into the load-bearing capacity of block structures. In Augenti et al. [6] studied the compressive behaviour of tuff block structures. In Lumantarna et al. [7] characterised the compressive strength and stress-strain relationship of old clay block structures. In Mojsilovic et al. [8] analysed high-story clay black walls and discussed their reliability. In Mojsilovic et al. [9] investigated the failure patterns and tensile strength of hollow clay blocks, observing brittleness and scattering in tensile strength due to initial cracking. In Zhai et al. [10] noted the increasing interest in concrete block structures and assessed their structural reliabilities. In Zhou et al. [11] investigated the compressive behaviour of hollow concrete block structures, identifying damage patterns and brittle failure. In Alvarez-Perez et al. [12] analysed the direct tensile behaviour and compressive strength of hollow concrete

blocks.

This article analyses the behaviour of hollow concrete blocks and structures built from them under compression. Individual blocks and structures with and without side supports are subjected to load-bearing tests to determine the effect of both: layering of the blocks on top of each other and placing them side by side. For the first time, the safety culvert design includes an opening that allows the flow of water and thus guarantees the main function of the culvert. Its size is expected to have a significant effect on the overall load capacity. Therefore, two variants, differing only in diameter of the circular opening, were produced, tested, and compared for load-bearing capacity. This work also presents a new design of the cellular structure, which has a thicker wall compared to the previous versions [2, 13, 14]. This modification facilitates the production and handling of blocks.

Numerical models are included to support and supplement the experimental data. Researchers have used various solvers to analyse the behaviour of hollow blocks and structures built from them under compression. For example, Kokal et al. [15] used finite element (FE) code LUSAS, and Zhu et al. [16] and Alvarez-Perez et al. [17] used FE code ABAQUS. In this study, the numerical model is constructed with the FE code ATENA [18] and is validated by the experiment. The model is then used for the parametric study of the effect of opening diameter, cell wall thickness, and concrete compressive strength on the overall load-bearing capacity. The FE code ATENA was specially designed for concrete and can simulate its real behaviour, e.g. cracking and crushing. At the same time, it has already been used in [19, 20] to analyse the quasi-static response of concrete structures designed to increase road safety.

2. Methodology

2.1. Experimental methodology

The experimental analysis consisted of two parts: load-bearing tests and the additional tests required for the determination of the mechanical properties of the base material, which will later be used in numerical simulations.

At first, the load-bearing capacity of individual blocks was examined. After that, three blocks were placed on top of each other, forming a column. Two types of columns were composed. One includes a circular opening and the other does not. Both compositions faithfully copied the vertical placement of the blocks in the resulting culvert and were subjected to quasi-static loads. Two versions of a column with a circular opening were tested, differing in the diameter of the opening. Later, side constraints were added to restrict the lateral movements of the blocks and simulate their placement side by side. Figure 1 shows the cellular structure of the blocks. The cell wall thickness is 20 mm. The dimensions of the cell are 190 × 35 mm (width × height).

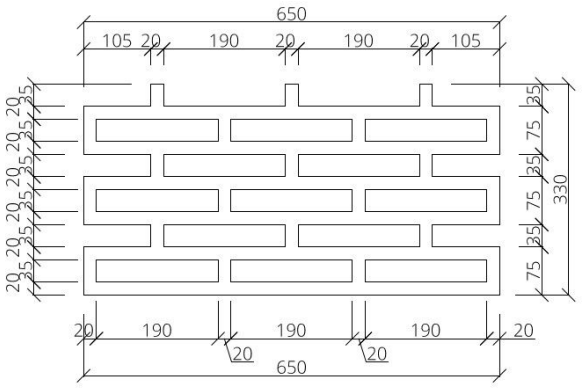

Figure 1. Plan view of a block with cellular structure; dimensions in mm.

In addition to the load-bearing tests, tests of the material used were also performed. Cube compressive strength was measured and used to pre-define the material model. The results of the three-point bending tests were used to refine and verify it.

2.1.1. Individual blocks

The individual blocks were subjected to quasi-static loading using a hydraulic loading device. The samples were loaded with increases in monotonic force at a rate of 0.36 MPa s^{-1}. The load generated by the hydraulic device was transferred using a steel block to the area of a square with a side of 300 mm.

The size of the steel block was selected according to the standard [21], depending on the contact area of the wheel and the possible spreading effect. This standard defines the load transfer area from the wheel to the structure as a square with a side length of 400 mm. In the context of the intended application of the deformation block, a smaller square area with a side length of 300 mm was chosen, as a smaller spreading height is expected than for bridge structures. The height of the steel block was 40 mm, which should be large enough to distribute the load evenly based on our experience and observations.

An 8 mm thick rubber interlayer was inserted between the steel block and the sample. The width of all blocks was 650 mm and their depth was 330 mm. Three types of blocks were tested: a low block with a cast top (10 mm thick board), see Figure 2 (a), a low block without a cast top, see Figure 2 (b), and a high block without a cast top, see Figure 2 (c). To demonstrate the repeatability of the experiment, the low-block tests were performed three times under identical conditions and the high-block test four times. The height of the higher block was 350 mm. The height of the low blocks was 200 mm. During the tests, the maximum achieved force was recorded as well as the loading force, at which there was a sudden reduction in load capacity.

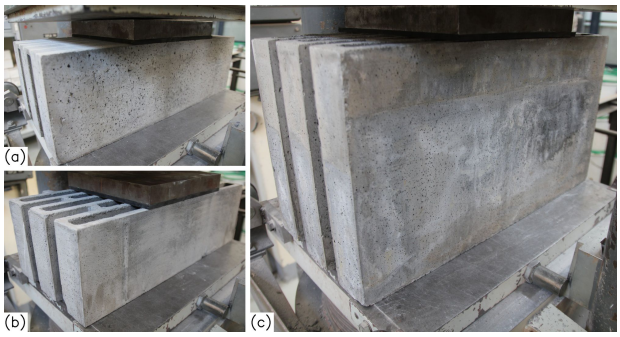

FIGURE 2. Blocks tested: a low block with a cast top (a), a low block without a cast top (b), and a high block without a cast top (c).

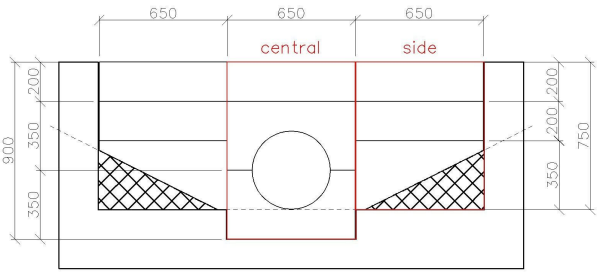

FIGURE 3. Block location and column composition in a safety culvert; dimensions in mm.

2.1.2. COLUMNS

The individual blocks are stacked on top of each other during the construction of the resulting culvert and thus create two types of columns; see Figure 3. The side column consists of a high block, a low block, and a low block with a full-cast top; see Figure 4 (a). The total height of the side column is 750 mm. The central column consists of two mirror-inverted high blocks with a semicircular water drain opening and one low block with a full-cast top, see Figure 4 (b). The total height of the central column is 900 mm. The response of two variants of the central column was examined, differing in the diameter of a circular hole: one had a diameter of 475 mm, the other 430 mm. A geotextile is inserted between the individual blocks and an 8 mm rubber layer is placed on top of the columns. The same compositional procedure was followed when preparing samples for laboratory tests. A square steel plate with a side length of 300 mm was placed on the rubber layer to distribute the load generated by the hydraulic loading machine. The experiment was controlled by deformation and the loading speed was $0.008\,\mathrm{mm\,s^{-1}}$. The force produced by the hydraulic loading device and the displacement of its moving part were recorded.

To verify the repeatability of the experiments, the side column load tests were performed four times, the central column with a 475 mm diameter opening three times, and the central column with a 430 mm diameter opening two times. The third sample with a 430 mm diameter opening was adhesed to the floor to limit its lifting during loading. In the resulting culvert, the columns will be placed right next to each other, which will prevent their lateral deformation and probably increase their load-bearing capacity. To match the conditions of a laboratory test closer to reality, the lateral deformation of the samples was restricted in the remaining tests.

Figure 4 also shows the test setup with side supports. Steel U-profiles type UPN200 were placed on the sides of the columns and fastened to each other with M16 threaded rods and nuts. The nuts were tightened by hand only to prevent pre-stress being introduced into the sample. The tests were carried out under identical conditions three times for each type of column with side supports. Due to the lack of blocks, the side column with side supports; see Figure 4 (d), also contained blocks cracked by a full-scale vehicular impact. These cracks visible to the naked eye were in the upper block; see Figure 5. The results of the vehicular crash test are not discussed in this contribution.

2.1.3. MATERIAL CHARACTERIZATION

The mechanical properties of the base material were determined experimentally using conventional procedures. The compressive cube strength was measured for bricks with a side length of 150 mm in a hydraulic loading machine using monotonic increments of load at a speed of $0.36\,\mathrm{MPa\,s^{-1}}$. The samples were tested at different time intervals after production to capture concrete strength development in time. These time periods were 2 hours, 20 hours, 200 hours (8 days), 336 hours (14 days), 672 hours (28 days), 1008 hours (42 days), 1344 hours (56 days), and 2000 hours (83 days) from the production. For each case, at least three similar samples were tested to prove the repeatability of the experiments. The samples were cured at an ambient temperature of 21 °C and relative humidity of 50 %. The modulus of rupture in the three-point bending test was measured for prismatic samples with dimensions of 40 × 40 × 160 mm (width × height × length) and a clear span of 100 mm. The test was performed under identical conditions eight times to demonstrate the repeatability of the experiment.

2.2. NUMERICAL METHODOLOGY

The numerical model was constructed with the finite element code ATENA [18] and validated by the experiment. The selected software was specially designed for concrete and calculates all properties of the material according to compressive strength. It can simulate a real behaviour of concrete, e.g., cracking and crushing of concrete.

To save computational time, only the central column was modeled, which was identified by experimental analysis as the weakest of the two columns. The validated model was used for the parametric study of the effect of the opening diameter, cell wall thickness,

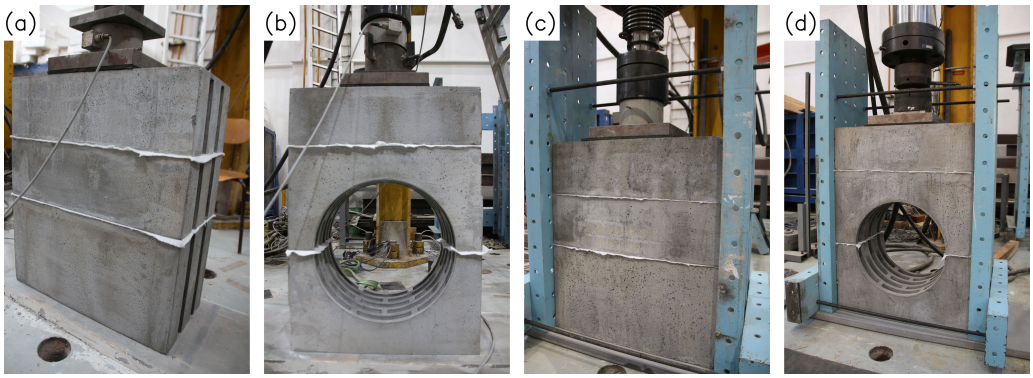

Figure 4. Columns with free boundary: a side column (a) and a central column (b); and columns with side deformation constraints: a side column (c) and a central column (d).

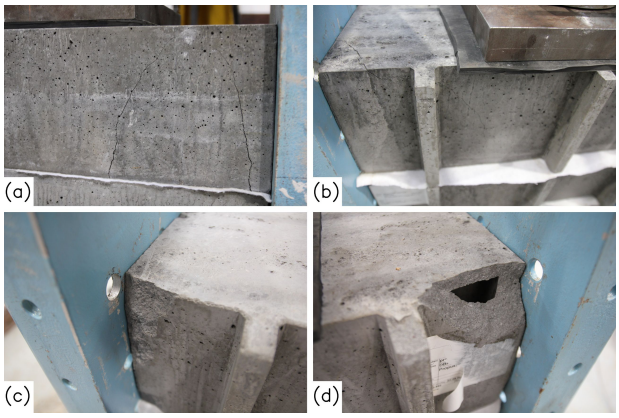

Figure 5. Pre-cracks visible to the naked eye in the upper blocks of side columns with side supports: two horizontal cracks in the front face of the first tested sample (a), cracked right rear corner of the second tested sample (b), cracked right rear corner of the third tested sample (c), and cracked left rear corner of the third tested sample (d).

and concrete compressive strength on the load-bearing capacity of the columns.

2.2.1. Model description

The threaded rods were discretised using beam elements. For the other parts of the model, solid elements were employed. For concrete blocks, brick elements with a side length of approximately 35 mm and linear basis functions are used. For the remaining 3D parts, brick elements with a side length of approximately 50 mm and quadratic basis functions are used. These element sizes proved to be a good compromise between simulation accuracy and computational time. Figure 6 shows the meshes used. Interface elements with zero thickness were used to model contacts between surfaces.

The interface elements were used together with the Interface Material Model. The material model is based on the Mohr-Coulomb criterion with an ellipsoid in the tension regime. The ellipsoid intersects the normal axis at tensile strength (f_t) with the vertical tangent and the shear axis at the defined value of cohesion (c) with the tangent equivalent to the negative value of a coefficient of friction ($-\phi$), see Figure 7. When the stress in an interface element meets the failure condition, the failure surface collapses to a residual surface. The residual surface corresponds to dry friction.

The concrete blocks were stacked on top of each other, with geotextiles inserted between the individual blocks. Tensile strength (f_t) and cohesion (c) of this contact can be considered negligible and, therefore, very small values were used; see Table 1. According to [18], it is recommended to always set the parameters f_t, c, and ϕ higher than zero. The friction coefficient (ϕ) between two concrete surfaces ranges from 0.5 to 0.9 [22]. The average value of this range is used in the numerical models; see Table 1. It was also verified that using other values in this range had no or negligible effect on the results. Future research will further evaluate and experimentally confirm the friction coefficient.

Figure 8 shows a typical behaviour of the interface model in tension and shear. The K_{nn} and K_{nn}^{min} denote the initial and minimal normal stiffness, respectively. Similarly, K_{tt} and K_{tt}^{min} are the initial and minimal shear stiffness.

The value of the normal (K_{nn}) and shear (K_{tt}) interface stiffness between two concrete parts, according to the experience of the authors and developers of the ATENA solver, is generally in the range of 2×10^6 to 2×10^8 MN m^{-3}. Table 1 shows the set of input values for each interface. The realisation of the contact between individual concrete blocks was the same during the experiments. However, during the development of the numerical model, it became clear that the usual value of shear stiffness (K_{tt}) between the middle and upper blocks artificially increases the shear interaction of these blocks, which, as a result, increases the bearing capacity of the column. The shear stiffness of this interface was significantly reduced to allow for the desired slip between the two blocks. A similar situation occurred later during the validation of the model with lateral supports at the interface between the concrete column and the steel profiles that form the lateral supports. Therefore, reduced shear stiffness

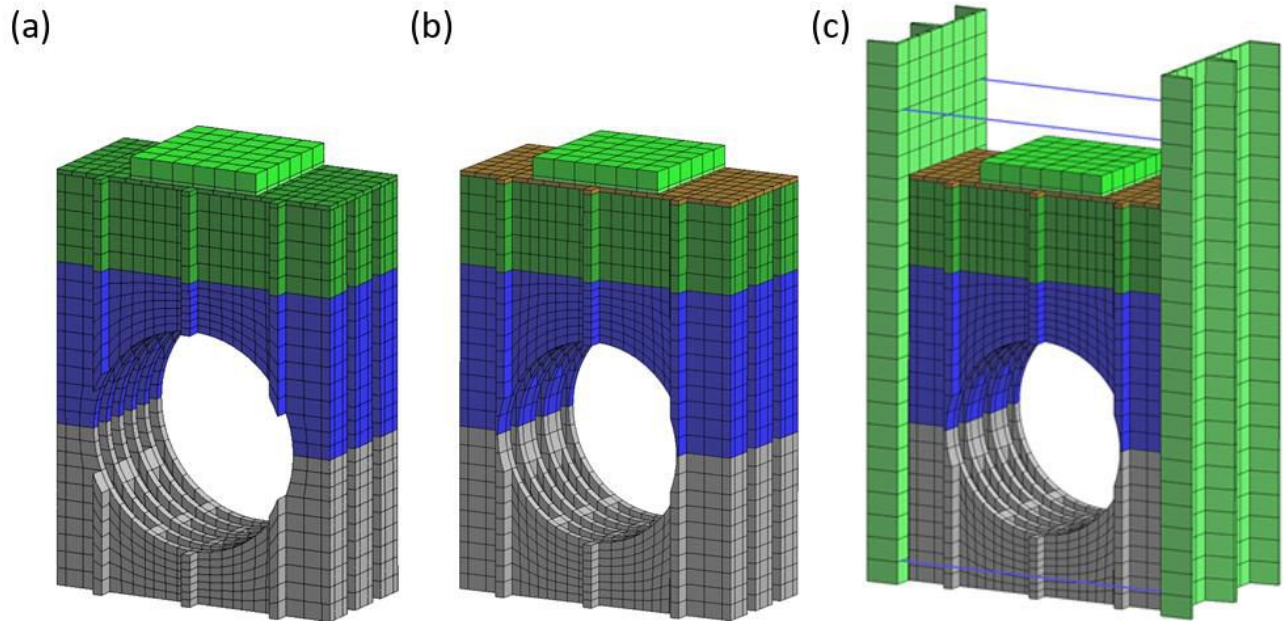

FIGURE 6. Finite element meshes of the three considered models for model validation: the free-standing central column with an opening diameter of 475 mm (a), the free-standing central column with an opening diameter of 430 mm (b), and the central column with an opening diameter of 430 mm and side supports (c).

Surface 1 **Surface 2**	**Floor** **Lower block**	**Lower block** **Middle block**	**Middle block** **Upper block**	**Blocks** **Side support**
c [MPa]	0.001	0.001	0.001	0.001
ϕ [–]	0.7	0.7	0.7	0.7
f_t [MPa]	0.0001	0.0001	0.0001	0.0001
K_{nn} [MPa m^{-1}]	2×10^7	2×10^7	2×10^7	2×10^7
K_{tt} [MPa m^{-1}]	2×10^6	2×10^6	20	20
K_{nn}^{min} [MPa m^{-1}]	0.001	200	2×10^4	0.001
K_{tt}^{min} [MPa m^{-1}]	200	2×10^4	0.1	0.1

TABLE 1. Input parameters used with the interface material model for different contacts.

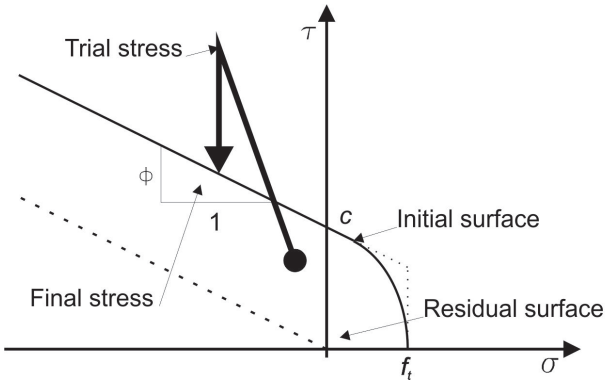

FIGURE 7. A failure surface of the interface model [18].

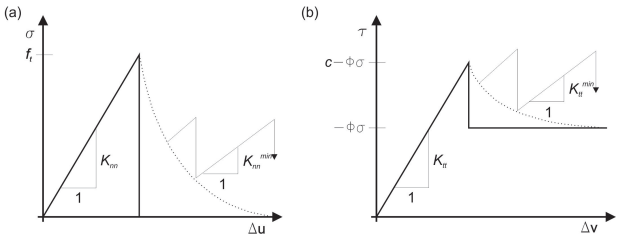

FIGURE 8. A typical behaviour of the interface model in (a) tension and (b) shear [18].

of the same value was also used for this interface.

The minimal normal (K_{nn}^{min}) and shear (K_{tt}^{min}) stiffness parameters are used only for numerical purposes to maintain the positive definiteness of the global equation system after the failure of the interface element. Theoretically, after the interface failure, the stiffness of the interface should be zero; i.e. the global stiffness will become indefinite. Therefore, the values should be set low enough not to artificially increase the bearing capacity but high enough to maintain the stability of the calculation. The parameters K_{nn}^{min} and K_{tt}^{min} listed in Table 1 were determined based on the previous experience of the authors and preliminary simulations to meet both of these criteria.

The Fracture-Plastic Constitutive Model type "CC3DNonLinCementitious2" from the ATENA material library simulated the concrete behaviour. It can be used to simulate cracking, crushing under high

Parameter	Symbol	Unit	Value
Young's modulus	E	[GPa]	40.44
Poisson's ratio	ν	[–]	0.2
Compressive cylinder strength	f_c	[MPa]	-66.5
Tensile strength	f_t	[MPa]	4
Fracture energy	G_f	[N m^{-1}]	60
Plastic strain at compressive strength	ε_{cp}	[–]	-0.00119
The onset of the nonlinear behaviour	f_{c0}	[MPa]	-9.06

TABLE 2. Input parameters used with the fracture plastic constitutive model for concrete blocks.

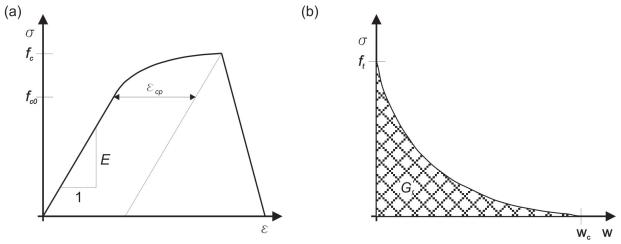

FIGURE 9. A typical behaviour of the fracture-plastic constitutive model in (a) compression and during the (b) tensile softening.

	E [GPa]	ν [–]	Eff cross-section [mm^2]
Side supports	200	0.3	–
Load-distributing plate	200	0.3	–
Threaded rods	200	–	157
Rubber layer	0.0005	0.46	–

TABLE 3. Input parameters used with the linear elastic model for different parts.

confinement, and crack closure due to the crushing of the material in other directions. The model combines models for tensile and compressive behaviour using the strain decomposition method defined in [23]. The combined algorithm makes it possible to develop and formulate the two models separately. It handles when both model failure surfaces are active and also when physical changes, such as cracked closures, occur.

Figure 9 shows the compressive hardening/softening plasticity model incorporated. Table 2 shows the input parameters. The compressive cylinder strength (f_c), Young's modulus (E), Poisson's ration (ν), plastic strain at the compressive strength (ε_{cp}), and the onset of nonlinear behaviour (f_{c0}) were generated using the measured compressive cube strength and the ATENA software preprocessor.

The fracture model in the tensile regime is based on the classical orthotropic smeared crack formulation and the crack band model. It uses the Rankine failure criterion and tensile softening; see Figure 10. In Figure 10, w_c is the maximum crack opening that can be evaluated using Equation 1 [18]:

$$w_c = 5.14\frac{G_f}{f_t}\,, \tag{1}$$

where G_f is the fracture energy and f_t is the tensile strength. Because the direct tensile test was not conducted, these two input parameters had to be determined using the data measured during the three-point bending test. A corresponding numerical model was constructed using the pairs of these two parameters, which were found to obtain the experimentally determined modulus of rupture; see Figure 10. The obtained pairs of parameters were subsequently inserted into the models of the columns, and the fracture energy G_f =60 N m^{-1} was chosen as the most suitable. To achieve even better agreement with the experiment, the tensile strength was reduced to 4 MPa. The difference in tensile strength could be due to the size effect or because the same casting procedure is not followed when producing samples of different sizes.

Steel or rubber parts were assigned a linear elastic material model with the parameters listed in Table 3. Movement of the lower surface of the interface elements between the concrete block and the floor of the laboratory is not allowed in any direction. A node at the top and bottom of each side support was also fixed to ensure the stability of the model. The load is generated by prescribing the motion of a node in the centre of the top surface of the load-distributing steel plate.

2.2.2. PARAMETRIC STUDY

The validated model was used for the parametric study of the effect of the opening diameter, cell wall thickness, and concrete compressive strength on the central column load-bearing capacity. The response of columns with opening diameters of 250 mm, 300 mm, 350 mm, 375 mm, 400 mm, 430 mm, and 475 mm was investigated. In the rest of the parametric studies, a constant hole diameter of 430 mm was considered.

During the study on the effect of cell wall thickness on the column load-bearing capacity, the thickness of the cell wall varied and all other internal dimensions varied accordingly to maintain the original proportions of the dimensions of the cellular structure. The external dimensions of the columns remained similar. Figure 11 shows a plan view of different cellular structures. The relevant dimensions are given in Table 4.

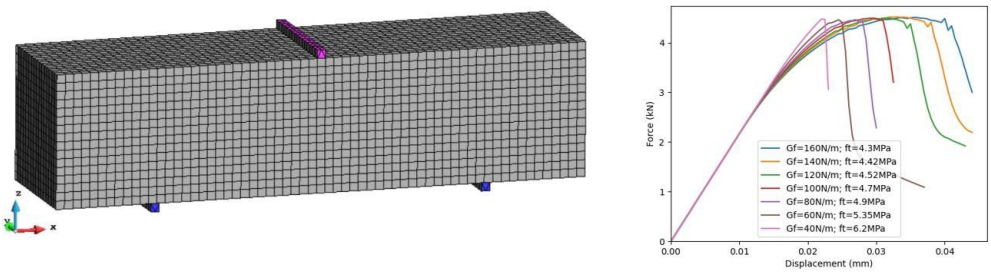

FIGURE 10. Numerical model of the three-point bending test for G_f and f_t parameter sensitivity studies.

Cell wall thickness [mm]	**width [mm]**	**height [mm]**	**Block width [mm]**	**height [mm]**	**Number of cells per width [–]**	**height [–]**
10	96	17	646	324	6	12
20*	190*	35*	650*	330*	3*	6*
30	280	54	650	336	2	4

* original design

TABLE 4. Dimensions of cellular structures considered during the parametric study.

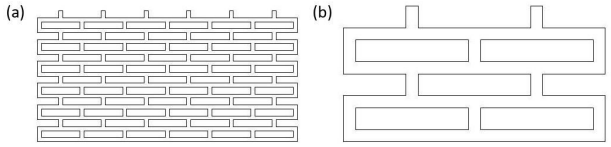

FIGURE 11. A plan view of cellular structures considered during the parametric study: a cell wall thickness of (a) 10 mm; (b) 30 mm.

Due to the fact that the used base material showed a wide range of strengths 28 days after the production, the effect of compressive strength on the load-bearing capacity of the columns was studied. The response of columns made of high-performance concrete with a compressive cube strength ranging from 50 MPa to 90 MPa with a step of 10 MPa was investigated. The remaining parameters of the Fracture-Plastic Constitutive Model, except for tensile strength and fracture energy, were again generated by the ATENA programme from the compressive cube strength. The tensile strength f_t^{new} was obtained using Equation (2):

$$f_t^{new} = \frac{f_t^{76.88}}{f_{t,gen}^{76.88} \times f_{t,gen}^{new}}, \tag{2}$$

where $f_t^{76.88}$ is the tensile strength used in the validated models, $f_{t,gen}^{76.88}$ is the tensile strength generated by the ATENA preprocessor for the compressive cube strength of 76.88 MPa, and $f_{t,gen}^{new}$ is the tensile strength generated by the ATENA preprocessor for the compressive cube strength studied. Similarly, the fracture energy G_f^{new} was obtained using Equation (3):

$$G_f^{new} = \frac{G_f^{76.88}}{G_{f,gen}^{76.88} \times G_{f,gen}^{new}}, \tag{3}$$

$f_{c,cube}$ [MPa]	50	60	70	76.88*	80	90
f_t [MPa]	3.02	3.48	3.85	4•	4.07	4.27
G_f [N m^{-1}]	55.7	57.7	59.2	60•	60.8	61.9

* measured value, • validated value

TABLE 5. Tensile strength (f_t) and fracture energy (G_f) considered in the parametric study on the effect of the compressive cube strength ($f_{c,cube}$).

where $G_f^{76.88}$ is the fracture energy used in the validated models, $G_{f,gen}^{76.88}$ is the fracture energy generated by the ATENA preprocessor for the compressive cube strength of 76.88 MPa, and $G_{f,gen}^{new}$ is the fracture energy generated by the ATENA preprocessor for the compressive cube strength studied. The tensile strength and fracture energy for each compressive cube strength considered are listed in Table 5.

3. RESULTS

3.1. MEASURED DATA

3.1.1. INDIVIDUAL BLOCKS

Before the maximum load capacity of the individual blocks was recorded, there was a sudden decrease in the load capacity of each block, after which the load force began to increase again. These values were also recorded and are shown in Table 6. The values of the maximum force are given in Table 7. Both values were highest for the high block. The lowest load-bearing capacity was recorded for a low block without a fully cast top. In contrast, the load-bearing capacity of

Block	Test 1	Test 2	test 3	Test 4	Average	Dev.
Low with a cast top	650	620	620	–	630	17
Low without a cast top	–	670	770	–	720	71
High without a cast top	980	1080	770	1140	993	162

Table 6. The force recorded just before a sudden reduction in the load-bearing capacity of blocks and its standard deviation (Dev.). Units are kN.

Block	Test 1	Test 2	Test 3	Test 4	Average	Dev.
Low with a cast top	1475	1535	1780	–	1597	162
Low without a cast top	1150	1490	1330	–	1323	170
High without a cast top	1350	1750	1570	1630	1575	168

Table 7. The maximum force recorded during a quasi-static test of individual blocks and its standard deviation (dev.). Units are kN.

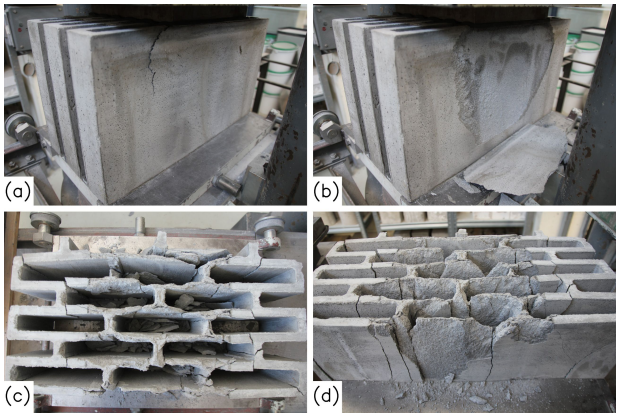

Figure 12. Phases of block collapse without a cast top: (a) A crack is formed in the sample near the edge of the steel plate; (b) a thin layer of concrete detaches from the flat wall; (c) material crushing below the steel plate; (d) formation of vertical cracks.

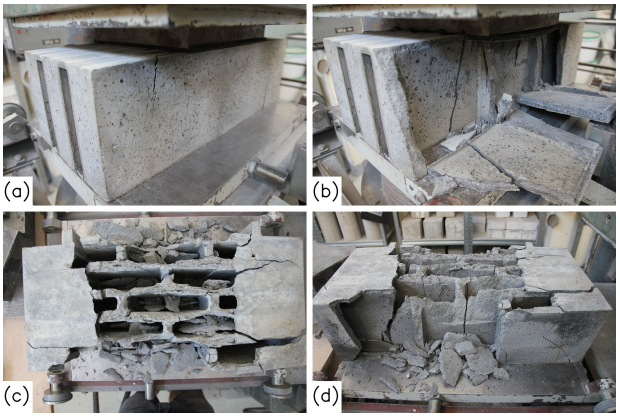

Figure 13. Phases of block collapse with a cast top: (a) A crack is formed in the sample near the edge of the steel plate; (b) an entire flat wall of the block fells off; (c) material crushing below the steel plate; (d) formation of vertical cracks.

a low block with a full cast top was comparable to that of a high block. This indicates that the cast top plate significantly increases the quasi-static bearing capacity of the block.

The collapse of all examined blocks was similar. In blocks without a cast top, cracks formed near the edges of the steel plate, see Figure 12 (a), probably due to the concentration of shear stress. Subsequently, a thin layer of concrete was detached from the flat side of the block, see Figure 12 (b). Later, the material under the steel plate was crushed, which was associated with pushing this plate into the block. With increasing load force, the material was further crushed, see Figure 12 (c), and vertical cracks were formed, see Figure 12 (d), until the maximum load capacity of the block was reached.

The collapse of the block with the cast top was similar. However, after the formation of cracks near the steel plate, see Figure 13 (a), instead of only a thin layer of concrete detaching the entire flat wall of the block fell off, see Figure 13 (b). The rest of the collapse was again similar to that of the blocks without a cast top: Material crushing, see Figure 13 (c), associated with pushing the steel plate into the block and forming vertical cracks, see Figure 13 (d), was observed.

3.1.2. Columns

Figure 14 (a) shows the dependence of the loading force on the displacement during the test of the side column. Figures 14 (b) and 14 (c) show the dependence of the loading force on the displacement during the test of the central column with a different opening diameter and boundary conditions, respectively. The maximum recorded forces are given in Table 8.

The load-bearing capacity of the central column was significantly lower than that of the side column and can thus be described as the weakest part of the safety culvert. This significant difference was due to the presence of a circular opening in the central column. Cracks form in the mid-span of both blocks with a semicircular opening. The resulting halves of the blocks are pushed to the sides. When the opening diameter is decreased, the force required to fracture

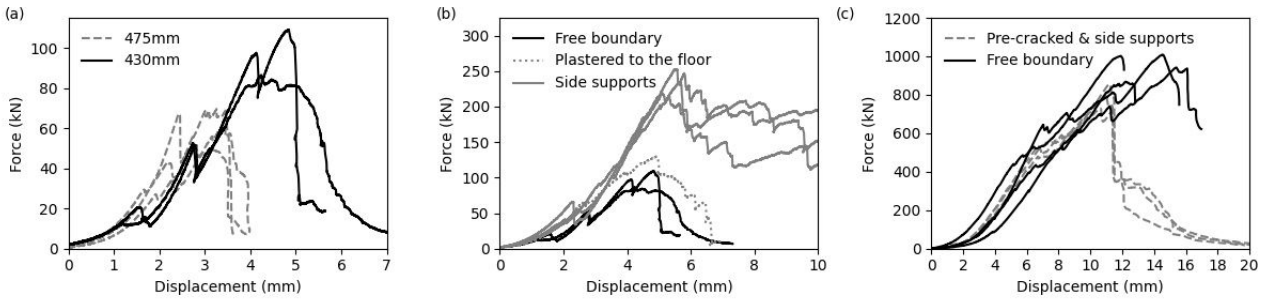

FIGURE 14. The dependence of the loading force on the displacement during the test of (a) the side column, (b) the central columns with different opening diameters, and (c) the central columns with different boundary conditions.

Column	Test 1	Test 2	Test 3	Test 4	Average	Dev.
Central ∅475mm	52	70	63	–	62	9
Central ∅430mm	86	109	–	–	98	16
Central ∅430mm •	130	–	–	–	130	–
Central ∅430mm *	215	252	234	–	234	19
Side *°	729	804	855	–	796	63
Side	942	1008	868	1002	955	65

• plastered to the floor, * side supports, ° pre-cracked sample

TABLE 8. Maximum force recorded during a quasi-static test of columns and its standard deviation (dev.). Units are kN.

the column increases, and so does the load-bearing capacity. The maximal vertical displacement also significantly increases.

The adhesion of the lower block of the central column to the floor limited the central part of the lower block from being lifted. This led to a slight increase in maximum force, while the maximum vertical displacement remained similar. Restraining the lateral deformation led to a significant increase in maximum force. The maximum vertical displacement increased more than six times compared to free-standing columns.

The presence of side supports also increased the maximum vertical displacement of the side column; see Figure 14. The sudden collapse observed in the free-standing side column was eliminated and a gradual decrease in the loading force was recorded, along with an increase in vertical displacement. In contrast to the central column, the lowest maximum force was recorded for the side column with side supports. However, this was most likely not due to the presence of side supports, but because these columns were made up of precracked blocks.

The results suggest that the presence of the side supports affects the maximum value of the force recorded for the central column more than the side column. Unfortunately, this conclusion cannot be fully supported by the results of the measurement carried out, as the response of the undamaged side columns with side supports was not examined. On the contrary, it can be stated with considerable certainty that the presence of side supports eliminates sudden collapse and prolongs vertical deformation.

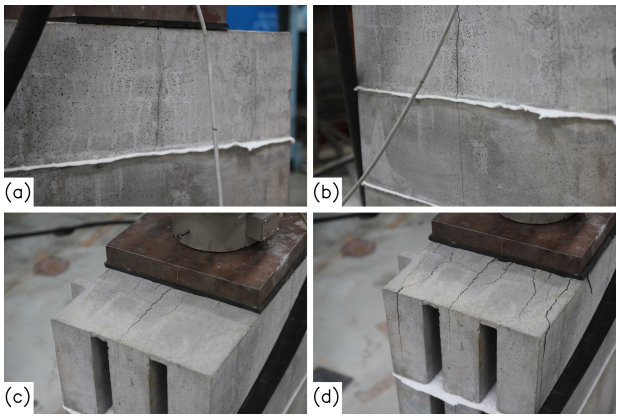

FIGURE 15. Phases of side column collapse: (a) A first crack forms in the upper block; (b) the crack continues into the middle block; (c) horizontal cracks form on the top plate; (d) the cracks open and the steel plate is pushed into the block.

During the loading of the free-standing side column, a vertical crack was first formed in the upper block, see Figure 15 (a), followed by a vertical crack in the middle block, see Figure 15 (b). Later, a crack formed in the lowest block. With increasing displacement, more vertical cracks appeared in most cases. The ones in the upper block were significant, one in the middle and two at the edges of the steel plate. Furthermore, horizontal cracks formed in the cast top of the upper block, see Figure 15 (c), the cracks opened and the steel plate was pushed into the block, see Figure 15 (d), until an absolute collapse occurred. The absolute

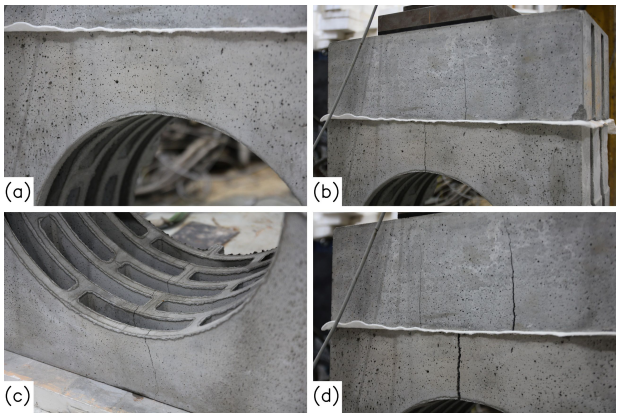

Figure 16. Phases of free-standing central column collapse: (a) A first crack forms in the mid-span of the arch in the middle block; (b) a crack forms in the upper block; (c) cracks forms in the mid-span of the arch in the lower block; (d) the cracks open and in the case of a block with an opening diameter of 475 mm, a second crack is formed in the upper block.

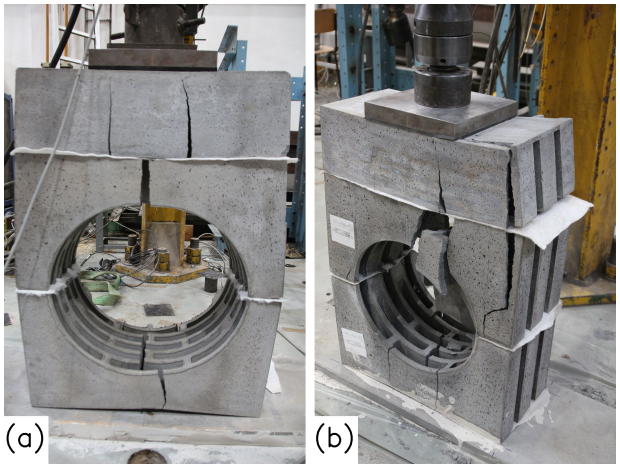

Figure 17. The cracks open until the complete collapse of the column occurs: (a) The free-standing column; (b) the column with the lower block adhesed to the floor.

collapse was characterised by the disintegration of the upper and most of the middle blocks. The lower block contained cracks but did not disintegrate.

The collapse of the side-supported side column was very similar to that of the free-standing one. Except for some of the first cracks formed near the preexisting cracks. Moreover, a sudden collapse was not observed; instead, the steel plate was further pressed into the sample.

During loading of the free-standing central column, the first crack formed in the middle block in the mid-span of the arch, see Figure 16 (a). Subsequently, a crack was also formed in the upper block, see Figure 16 (b), and in the lower block in the mid-span of the arch, see Figure 16 (c). In the case of a block with an opening with a diameter of 475 mm, another significant crack formed later in the upper block, see Figure 16 (d). All these cracks further opened under

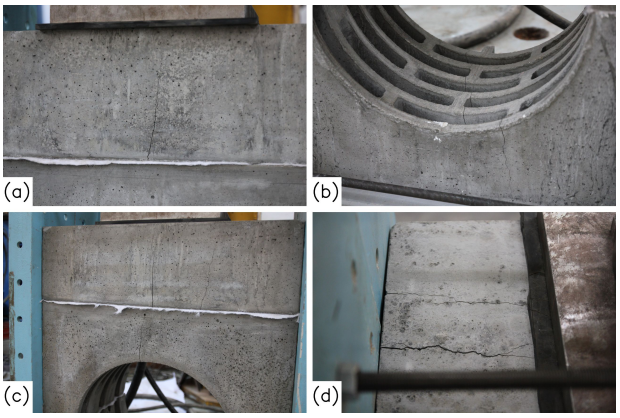

Figure 18. Phases of side-supported central column collapse: (a) First cracks form in the upper block; (b) a crack forms in the mid-span of the arch in the lower block; (c) a crack forms in the mid-span of the arch in the middle block; (d) horizontal cracks form on the top plate.

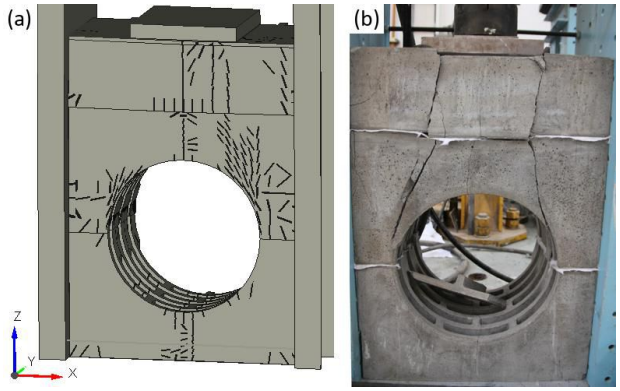

Figure 19. Cracks developed in the side-supported central column in (a) numerical and (b) experimental analysis.

the compression increments, see Figure 17 (a), until the complete collapse of the column occurred. The adhesion to the floor limited the lifting of the lower block and increased the formation of cracks in the upper parts of the column, but the collapse process was similar to that of a free-standing column, see Figure 17 (b).

The collapse of the side-supported central column differed in some aspects from that of the free-standing ones. In some aspects, it even resembled the collapse of the side column. The first crack formed in the upper block, see Figure 18 (a) followed by a crack in the bottom block in the mid-span of the arch, see Figure 18 (b), and a crack in the mid-span of the arch of the middle block, see Figure 18 (c). Cracks in the mid-spans no longer opened. Instead, horizontal cracks formed in the cast top of the upper block, see Figure 18 (d). In the upper block, two significant vertical cracks formed near the edges of the steel plate and progressed into the middle block, see Figure 19 (b). The sudden collapse was not observed; instead, the steel plate was further pressed into the sample.

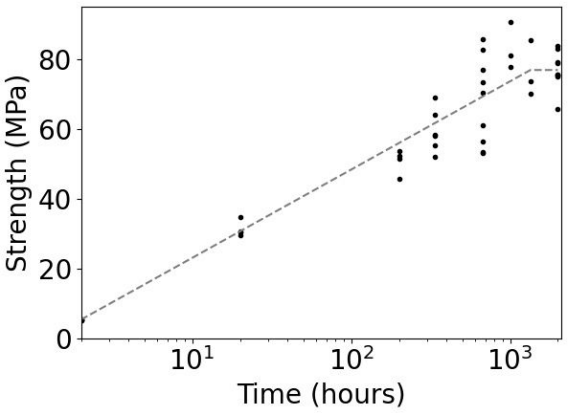

FIGURE 20. Time evolution of compressive cube strength of high-performance concrete with logarithmic curve approximation.

3.1.3. MATERIAL CHARACTERIZATION

Figure 20 shows the development of the concrete strength with time. The cubic compressive strength of the high-performance concrete used increased for 6 weeks after the sample production. The final compressive cube strength was determined, using three 8-week samples and nine 12-week samples, to be 76.88 MPa with a standard deviation of 5.98 MPa. The modulus of rupture was determined, using eight samples, to be 10.55 MPa with a standard deviation of 1.03 MPa.

3.2. COMPUTED DATA

3.2.1. MODEL VALIDATION

Figure 21 shows the comparison of the experimental and numerical results in terms of the evolution of the contact force. Brittle failure in bending tension in the middle of all concrete blocks was observed for both types of free-standing columns; see Figures 22 and 23. Flexural cracks are also present in the column with side supports; see Figure 19. However, because of the restricted lateral displacements, the cracks do not open and the column does not collapse. The final failure of the structure is observed much later by compressive crushing of the concrete at the base of the arch of the upper concrete block, where the parameter of the critical compressive plastic strain ($\varepsilon_{cp} = 0.00119$) is exceeded; see Figure 24.

3.2.2. PARAMETRIC STUDY

The load-bearing capacity and displacement at the maximum load force decrease as the opening diameter of the free-standing central column increases; see Figure 25 (a). The mode of failure gradually changes with increasing opening diameter from concrete crushing at the base of the middle block arch, i.e. the value of the equivalent plastic strain in a calculation step after the peak of the bearing capacity is greater than the parameter ε_{cp}, to the bending-tension failure in the middle of all blocks, i.e. the value of the equivalent plastic strain in a calculation step beyond the peak-bearing capacity is smaller than the parameter ε_{cp}; see Figure 26.

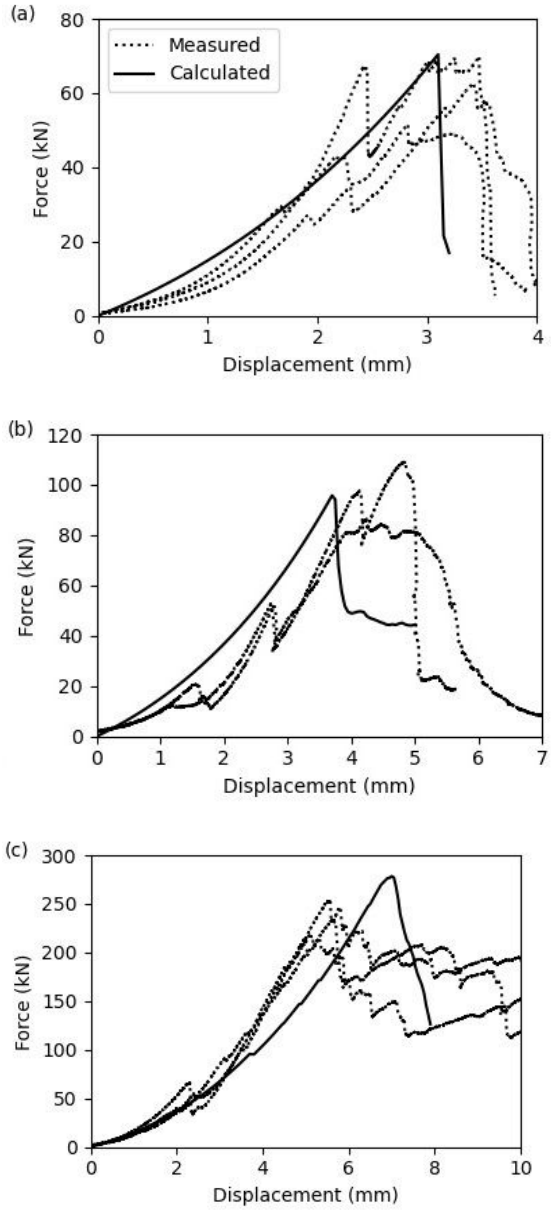

FIGURE 21. Validation of the computed and measured dependence of the loading force on the displacement acting on (a) a free-standing central column with an opening diameter of 475 mm, (b) a free-standing central column with an opening diameter of 430 mm, and (c) a central column with an opening diameter of 430 mm and side supports.

Figure 27 shows the force-displacement graphs for the central columns with different cell wall thicknesses. The difference in the response of the central column with or without side supports when decreasing the cell wall thickness to 10 mm is negligible. When the thickness of the cell wall increases to 30 mm, a decrease in stiffness is noticeable. However, the effect of cell wall thickening on the load-bearing capacity cannot be clearly established. The capacity of the side-supported

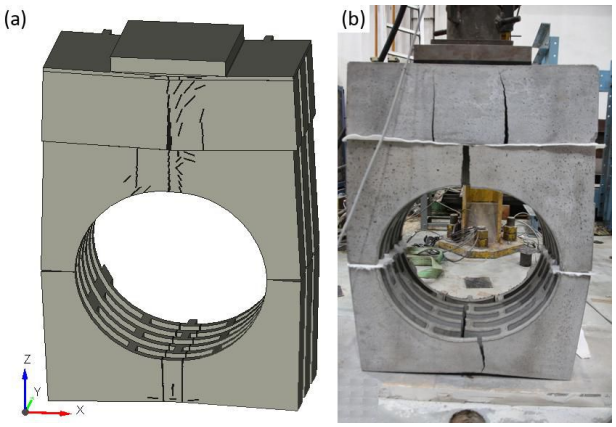

Figure 22. Cracks developed in the free-standing central column with an opening diameter of 475 mm in (a) numerical and (b) experimental analysis.

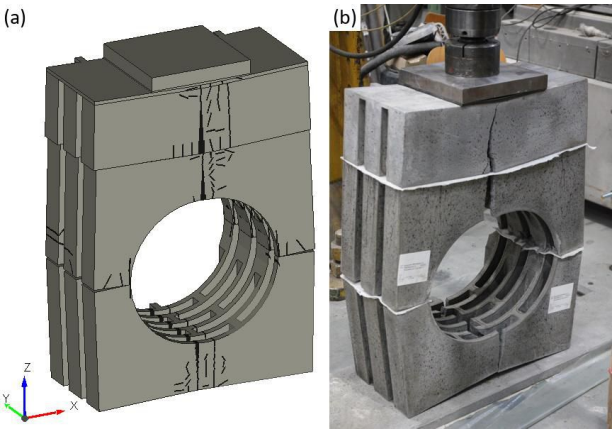

Figure 23. Cracks developed in the free-standing central column with an opening diameter of 430 mm in (a) numerical and (b) experimental analysis.

column increases by 10 % (from 95.7 kN to 105.9 kN), but decreases by 8 % (from 277 kN to 255.9 kN) for the free-standing column.

The load-bearing capacity and displacement at the maximum load force increase as the compressive cube strength increases; see Figure 25 (b). With an increase in the compressive cube strength by 80 % (from 50 MPa to 90 MPa), the bearing capacity of the free-standing column increases by 23 % (from 80.3 kN to 99 kN) and the bearing capacity of the side-supported column by 25.8 % (from 234 kN to 294.5 kN). The failure modes were similar for the material models with different input parameters.

4. Discussion

The computational-experimental research program was used to study the uniaxial compression behaviour of hollow high-performance concrete blocks with a brittle cellular structure. The developed numerical model was able to accurately predict the failure mode, including the crack distribution; see Figures 19, 22, and 23. The calculated and measured maximum forces are in good agreement; see Figure 21. The experimental and numerical methods were in 89 %, 98 %, and 84 % agreement for the maximum forces obtained for the free-standing central column with an opening diameter of 475 mm, the free-standing central column with an opening diameter of 430 mm, and the central column with an opening diameter of 430 mm and side supports, respectively.

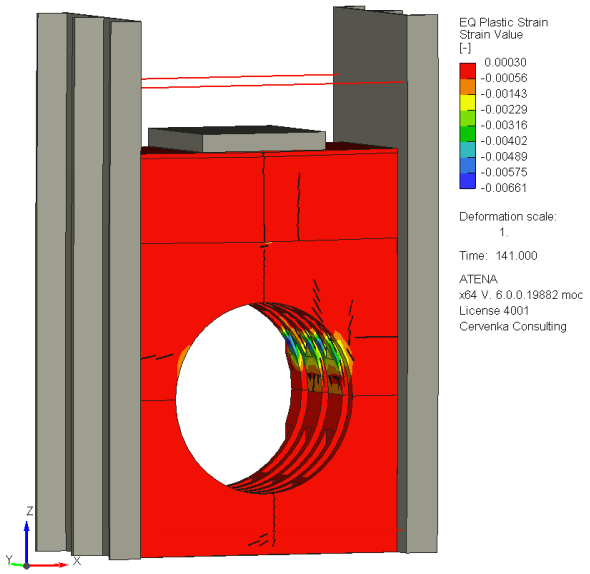

Figure 24. Equivalent plastic strain developed in the side-supported central column with an opening diameter of 430 mm.

The central column was identified as the weakest column in the safety culvert. The maximum force achieved in its load test was approximately ten times lesser than in the side column test; see Table 8. This significant difference was due to the presence of a circular opening in the central column. While in the case of the side column, the material was crushed and the load plate was pushed into the block, in the case of the side-supported central column, the cracks connected the edges of the load plate to an opening and the material under the load plate was pushed into the opening; see Figure 19.

The bearing capacity of the central column can be increased by strengthening the base material. However, the increase in the bearing capacity is not proportional to the increase in the strength of the base material, and such a strengthening could be economically unfeasible. According to a numerical parametric study, an increase in the compressive strength of the material by a factor of 1.8 will only increase the load-bearing capacity of the structure by approximately 1.2 times; see Figure 25 (b).

A much better option seems to be to reduce the water flow opening. By reducing its diameter below 400 mm and further, there is a significant increase in bearing capacity. The failure mode changes as the opening diameter decreases, from bending failure in the centre of the blocks to concrete crushing at the base of the central block arch. Up to a diameter of

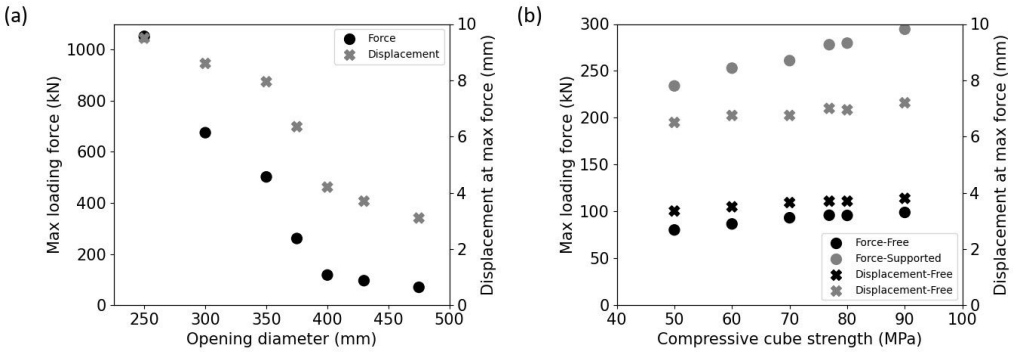

FIGURE 25. Load-bearing capacity and displacement at the maximum loading force of the free-standing central column with (a) different opening diameters or with (b) different compressive cube strength.

FIGURE 26. Crack pattern, deformation, and equivalent plastic strain developed in the free-standing central column with an opening diameter of (a) 250 mm, (b) 3000 mm, (c) 350 mm, (d) 375 mm, (e) 400 mm, (f) 430 mm, and (g) 475 mm.

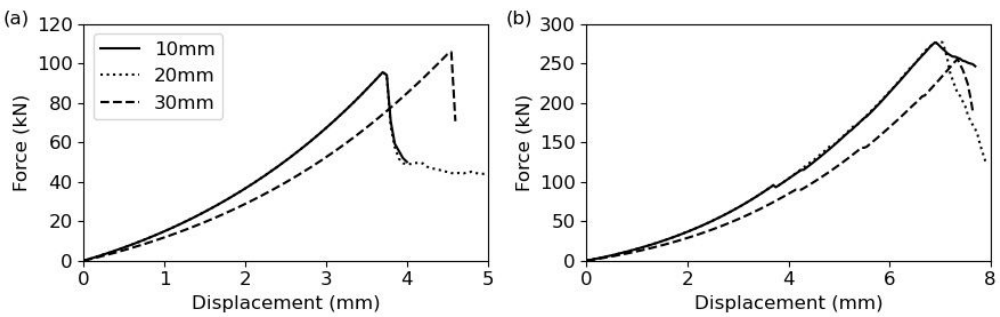

FIGURE 27. The dependence of the loading force on the displacement calculated for the (a) free-standing and (b) side-supported central columns with different cell wall thicknesses.

400 mm, the load capacity increased by approximately 0.64 kN per millimetre of diameter reduction. Thereafter, the load capacity increased almost ten times faster, at approximately 6.23 kN per millimetre of diameter reduction; see Figure 25 (a).

Reducing the cell wall thickness to 10 mm did not lead to an increase in bearing capacity; see Figure 27. The original design with a wall thickness of 20 mm remains a better option, for which better handling is expected due to the higher damage resistance, as well as an easier demoulding process due to a smaller friction surface. Details of block production, including demoulding, can be found in [2].

The column does not collapse suddenly if supported from the sides. Given that in the resulting culvert, the columns are placed next to each other, it can be assumed that a sudden collapse should not be recorded even during loading by passing vehicles, and the eventual sinking of the vehicle should be preceded by the formation of visible cracks.

Based on the observations made, it can be assumed that if a crack is formed in the culvert during its loading by passing vehicles, the first of these cracks will form in the upper layer of blocks, followed by a crack in the water flow opening. Therefore, it is necessary to monitor this part more closely during follow-up tests. If cracks appear, blocks with a modified design will be necessary for the replacement. This could be a block with a reduced opening diameter.

5. Conclusions

This study investigated the compression behaviour of a safety culvert made of high-performance hollow concrete blocks subjected to quasi-static loading. To the knowledge of the authors, the presented data are the first of their kind. The following inferences can be drawn from the study:

(1.) The developed numerical model was able to accurately predict the failure mode, including the crack distribution, and can be used in follow-up studies. The calculated maximum forces and vertical deformations were in good agreement with the measured data.

(2.) The load-bearing capacity of the central column was significantly lower than that of the side column and can thus be described as the weakest part of the safety culvert. This significant difference was due to the presence of a circular opening in the central column.

(3.) By decreasing the opening diameter, the maximal vertical displacement significantly increases, the force required to fracture the sample also increases, and so does the load-bearing capacity. The failure mode changes from bending stress failure in the centre of all blocks to concrete crushing at the base of the arch.

(4.) The difference in the response of the central column with or without side supports when decreasing the cell wall thickness to 10 mm is negligible. When increasing the thickness of the cell wall to 30 mm, a decrease in stiffness is noticeable. However, the effect of cell wall thickening on the load-bearing capacity cannot be clearly established.

(5.) The load-bearing capacity and the displacement at the maximum loading force increase as the compressive cube strength increases.

(6.) Attaching the sample to the floor with an adhesive limited the lifting of the central part of the lower block. This led to a slight increase in maximum force, while the maximum vertical displacement remained similar.

(7.) Restraining the lateral deformation of the central column resulted in a significant increase in maximum force, elimination of sudden collapse, and prolongation of vertical deformation. Flexural cracks that open during the loading of the free-standing central column do not open in the side-supported column.

(8.) The load-bearing capacity of its individual parts was tested under laboratory conditions. Future studies will be devoted to the response of the safety culvert to vehicle-induced loading in a real environment. Based on the observations made, it can be assumed that if a crack is formed in the culvert during its loading by passing vehicles, the first of these cracks will form in the upper layer of blocks, followed by a crack in the water flow opening. Therefore, it is necessary to monitor this part more closely during follow-up tests. If cracks appear, blocks with a modified design will be necessary for the replacement. This could be a block with a reduced opening diameter.

List of symbols

E Young's modulus [Pa]
G_f fracture energy [N m^{-1}]
K_{nn} initial normal stiffness [Pa m^{-1}]
K_{nn}^{min} minimal normal stiffness [Pa m^{-1}]
K_{tt} initial shear stiffness [Pa m^{-1}]
K_{tt}^{min} minimal shear stiffness [Pa m^{-1}]
c cohesion [Pa]
f_c compressive cylinder strength [Pa]
$f_{c,cube}$ compressive cube strength [Pa]
f_{c0} onset of nonlinear behavior [Pa]
f_t tensile strength [Pa]
w_c maximum crack opening [m]
ε_{cp} plastic strain at the compressive strength
ν Poisson's ratio
ϕ friction coefficient

Acknowledgements

This work was supported by the Technology Agency of the Czech Republic (grant number TH04010066). The au-

thors also acknowledge the assistance of students from the Experimental Center of the Faculty of Civil Engineering of the Czech Technical University in Prague who participated in the project as part of the internal Student Grant Competition (SGS23/053/OHK1/1T/11).

References

[1] T. Mičunek, Z. Schejbalová, D. Schmidt. Access bridge design measures for safety increase of road infrastructure. *Safety and Security in Traffic Preliminary Communication* **25**(6):543–554, 2013. https://doi.org/10.7307/ptt.v25i6.436

[2] P. Hála, R. Sovják, M. Frydrýn, T. Mičunek. Energy absorbing system made of high performance concrete. *Construction and Building Materials* **139**:64–80, 2017. https://doi.org/10.1016/j.conbuildmat.2017.02.048

[3] P. Hála, R. Sovják, T. Mičunek, et al. Fracture behaviour of ceramic blocks with thin-walled cellular structures under dynamic loadings. *Thin-Walled Structures* **122**:597–605, 2018. https://doi.org/10.1016/j.tws.2017.10.050

[4] P. Máca, R. Sovják, T. Vavřiník. Experimental investigation of mechanical properties of UHPFRC. *Procedia Engineering* **65**:14–19, 2013. https://doi.org/10.1016/j.proeng.2013.09.004

[5] M. Pigeon, R. Gagné, P.-C. Aïtcin, N. Banthia. Freezing and thawing tests of high-strength concretes. *Cement and Concrete Research* **21**(5):844–852, 1991. https://doi.org/10.1016/0008-8846(91)90179-L

[6] N. Augenti, F. Parisi. Constitutive models for tuff masonry under uniaxial compression. *Journal of Materials in Civil Engineering* **22**(11):1102–1111, 2010. https://doi.org/10.1061/(ASCE)MT.1943-5533.0000119

[7] R. Lumantarna, D. T. Biggs, J. M. Ingham. Uniaxial compressive strength and stiffness of field-extracted and laboratory-constructed masonry prisms. *Journal of Materials in Civil Engineering* **26**(4):567–575, 2014. https://doi.org/10.1061/(ASCE)MT.1943-5533.0000731

[8] N. Mojsilović, M. G. Stewart. Probability and structural reliability assessment of mortar joint thickness in load-bearing masonry walls. *Structural Safety* **52**:209–218, 2015. https://doi.org/10.1016/j.strusafe.2014.02.005

[9] N. Mojsilović. Tensile strength of clay blocks: An experimental study. *Construction and Building Materials* **25**:4156–4164, 2011. https://doi.org/10.1016/j.conbuildmat.2011.04.052

[10] X. Zhai, M. G. Stewart. Structural reliability analysis of reinforced grouted concrete block masonry walls in compression. *Engineering Structures* **32**(1):106–114, 2010. https://doi.org/10.1016/j.engstruct.2009.08.020

[11] Q. Zhou, F. Wang, F. Zhu, X. Yang. Stress–strain model for hollow concrete block masonry under uniaxial compression. *Materials and Structures* **50**:106, 2017. https://doi.org/10.1617/s11527-016-0975-5

[12] J. Álvarez-Pérez, M. Mesa-Lavista, J. H. Chávez-Gómez, G. Fajardo-San Miguel. Experimental investigation on tensile strength of hollow concrete blocks. *Materials and Structures/Materiaux et Constructions* **54**(4):164, 2021. https://doi.org/10.1617/s11527-021-01761-3

[13] P. Hála, R. Sovják, M. Munduchová, et al. High-load bearing deformation block made of UHPC. In *Second International Interactive Symposium on Ultra-High Performance Concrete*, vol. 2, pp. 1–2. Albany, NY, USA, 2019. https://doi.org/10.21838/uhpc.9657

[14] P. Hála, L. Nouzovský. Crashworthiness of brittle blocks as cushioning elements for fixed objects around traffic lanes. *Transportation Research Procedia* **55**:1042–1049, 2021. https://doi.org/10.1016/j.trpro.2021.07.076

[15] H. O. Köksal, C. Karakoç, H. Yildirim. Compression behavior and failure mechanisms of concrete masonry prisms. *Journal of Materials in Civil Engineering* **17**(1):107–115, 2005. https://doi.org/10.1061/(ASCE)0899-1561(2005)17:1(107)

[16] F. Zhu, Q. Zhou, F. Wang, X. Yang. Spatial variability and sensitivity analysis on the compressive strength of hollow concrete block masonry wallettes. *Construction and Building Materials* **140**:129–138, 2017. https://doi.org/10.1016/j.conbuildmat.2017.02.099

[17] J. Álvarez-Pérez, J. H. Chávez-Gómez, B. T. Terán-Torres, et al. Multifactorial behavior of the elastic modulus and compressive strength in masonry prisms of hollow concrete blocks. *Construction and Building Materials* **241**:118002, 2020. https://doi.org/10.1016/j.conbuildmat.2020.118002

[18] V. Červenka, D. Pryl, J. Červenka. *ATENA Program Documentation, Part 1: Theory.* Červenka Consulting s.r.o., 2021.

[19] F. Duchesneau, J.-P. Charron, B. Massicotte. Monolithic and hybrid precast bridge parapets in high and ultra-high performance fibre reinforced concretes. *Canadian Journal of Civil Engineering* **38**(8):859–869, 2011. https://doi.org/10.1139/L11-054

[20] M. Namy, J.-P. Charron, B. Massicotte. Structural behavior of bridge decks with cast-in-place and precast concrete barriers : Numerical modeling. *Jornal of Bridge Engineering* **20**(12):1–11, 2015. https://doi.org/10.1061/(ASCE)BE.1943-5592.0000751

[21] Eurokód 1: Zatížení konstrukcí - Část 2: Zatížení mostů dopravou. Úřad pro technickou normalizaci, metrologii a státní zkušebnictvý, Praha, 2018.

[22] Eurocode 2: Design of concrete structures - Part 1-1: General rules and rules for buildings. Comite Europeen de Normalisation, Brussels, 2005.

[23] R. De Borst. *Non-linear analysis of frictional materials.* Ph.D. thesis, Delft Univesity of Technology, Netherlands, 1986.